

PCCP

Accepted Manuscript



This is an *Accepted Manuscript*, which has been through the Royal Society of Chemistry peer review process and has been accepted for publication.

Accepted Manuscripts are published online shortly after acceptance, before technical editing, formatting and proof reading. Using this free service, authors can make their results available to the community, in citable form, before we publish the edited article. We will replace this *Accepted Manuscript* with the edited and formatted *Advance Article* as soon as it is available.

You can find more information about *Accepted Manuscripts* in the [Information for Authors](#).

Please note that technical editing may introduce minor changes to the text and/or graphics, which may alter content. The journal's standard [Terms & Conditions](#) and the [Ethical guidelines](#) still apply. In no event shall the Royal Society of Chemistry be held responsible for any errors or omissions in this *Accepted Manuscript* or any consequences arising from the use of any information it contains.

Structural Investigation of Resorcinol based Symmetrical Banana Mesogens by XRD, NMR and Polarization measurements

M. Kesava Reddy[‡], E. Varathan[†], B. Jacintha[#], Nitin P. Lobo^{a§}, Arun Roy^{#*},
T. Narasimhaswamy[†] and K. V. Ramanathan^{♦*}

ABSTRACT

Synthesis and structural characterization of two novel symmetrical banana mesogens built from resorcinol with seven phenyl rings linked by ester and imine with terminal dodecyl/dodecyloxy chain has been carried out. Density Functional Theory (DFT) has been employed for obtaining the geometry optimized structures, the dipole moments and ^{13}C NMR chemical shifts. The HOPM and DSC studies revealed enantiotropic B_2 and B_7 phases for the dodecyl and dodecyloxy homologs respectively. The powder X-ray studies of both the mesogens indicate the presence of layer ordering. The polarization measurements reveal an anti-ferroelectric switching for the B_2 phase of the dodecyl homolog whose structure has been identified as SmC_sP_A . The B_7 phase of the dodecyloxy homolog was found to be non-switchable. High resolution ^{13}C NMR study of the dodecyl homolog in its mesophase has been carried out. ^{13}C - ^1H dipolar couplings obtained from the 2-dimensional separated local field spectroscopy experiment were used to obtain the orientational order parameters of the different segments of the mesogen. Very large ^{13}C - ^1H dipolar couplings observed for the carbons of the central phenyl ring (9.7-12.3 kHz) in comparison to the dipolar couplings of those of the side arm phenyl rings (less than 3 kHz) are a direct consequence of the ordering in the banana phase and the shape of the molecule. From the ratio of the local order parameter values, the bent-angle of the mesogen could be determined in a straight forward manner to be 120.5° .

Keywords: Mesogen, Banana, XRD, ^{13}C NMR, Polarization, ^{13}C - ^1H dipolar couplings

1. Introduction

The banana mesogens are a distinct class of molecular materials exhibiting fascinating liquid crystalline properties.¹⁻⁵ The supramolecular organization leading to remarkable range of phase morphology and the formation of macroscopic chirality by spontaneous symmetry breaking are the two most important features of banana mesogens.⁶⁻⁸ Among the liquid crystalline phases exhibited by bent core molecules, the B_2 phase shows electro-optic switching. The B_2 phase has a lamellar structure with the long axes (the bow string axes) of the bent core molecules tilted with respect to the layer normal and the arrow axes of the molecules align perpendicular to the tilt plane giving rise to a layer polarization.⁶⁻⁸ This makes the layers chiral even though the molecules themselves are achiral. Depending on the relative orientations of the tilt and polarization vectors of adjacent layers, there are four possible structures in the B_2 phase.⁷ Another phase which is extensively studied because of its unique and characteristic textures is the B_7 phase. On slow cooling from the isotropic liquid to the B_7 phase, a variety of textures such as spiral, myelin like, accordion, checker-board, banana-leaf and circular domains were observed.^{3,7} Based on the observed layer modulations in the B_7 phase, a ferroelectric polarization modulated structure has been proposed for the phase. The key molecular designing parameters for the construction of banana mesogens include structural variations of the central parts, the lateral substituents, the linking groups, the terminal chains, and the number of rings as well as the bent-angle between the wings.^{1,4,9-11} As a consequence, a large amount of work dealing with structural variations and their influence on mesophase properties has been reported in literature.¹⁻¹⁶ For instance, it is observed that the increase of bent-angle to 140° or more would result in typical mesophases formed for calamitic molecules, such

as N, SmA, SmC, possibly in combination with banana phases.^{9,17} Further, the molecular conformational changes with the temperature *i.e.* the bending angle decreases with decreasing temperature.¹⁷ Additionally, the length as well as the chemical nature of the terminally attached hydrocarbon chains influences the type of mesophases and their phase sequence.⁴ In the light of these established molecular features, the current emphasis is placed more on understanding molecular level organization and its relation to molecular structure besides the synthesis of new molecules. Among many instrumental methods employed for arriving at the molecular organization, in recent years, high resolution solid state ²H and ¹³C NMR spectroscopy has attracted the attention of many researchers.¹⁷⁻²¹ Experiments in the mesophase have been carried out both on static samples and with MAS. Weissflog *et.al.*¹⁷ employed ¹³C NMR experiments in the banana mesophase to obtain the molecular structure, orientational order and the bent-angle and its variation with temperature. Watanabe *et.al.*¹⁸ utilized ¹³C CP MAS experiments in the B₄ mesophase to understand the origin of the twisted helical system. Walba *et.al.*¹⁹ also used the ¹³C CP MAS experiments to extract the information about the molecular organization in the banana mesophases. Dong *et.al.*²⁰ exploited ¹³C NMR spectroscopy for the determination of order and dynamics of different structural fragments of the banana mesogens. Veracini *et.al.*²¹ based on their ²H and ¹³C NMR experiments proposed a model considering the existence of more than one conformation and also explained the difficulty in orienting the banana mesogens.

In this work, we report the synthesis and structural characterization of resorcinol based symmetrical seven phenyl ring banana mesogens with terminal dodecyl/dodecyloxy chain. Resorcinol is the most widely used central unit for bent-core mesogens which exhibit banana as well as conventional smectic or nematic

phases.^{22, 23} The linking unit between the central phenyl ring and the side arm core is chosen to be the ester group since the imine linkage has less conformational flexibility and is less polar than an ester unit. Thus the imine linkage is less favoured at the central core unit for the generation of banana phases. Further, the imine linking group is more conjugative and less sterically challenging than the ester analogue, which leads to higher clearing points.^{1,9} The characterization of banana mesophases assumes greater significance since subtle change in the molecular structure, dramatic change in mesophase properties are often noticed. The presence of seven phenyl rings in the synthesized molecules ensured the banana phases. Besides the mesophase properties, the electro-optic measurements of synthesized molecules have been carried out. We observe that despite the structural similarity, the mesogens reveal many differences owing to the addition of just an oxygen atom on either side. Further, we also employ the 2D separated local field (2D-SLF) NMR spectroscopy for establishing the banana topology. This approach has a significant advantage over the use of just the ^{13}C chemical shifts. Due to non-uniform alignment of the director in these phases, the spectral lines of a static sample oriented in a magnetic field tend to have large line-widths. This leads to loss of information arising from limited resolution due to overlap of important resonances.^{17b} The 2D approach presented here addresses this problem by improving the resolution in the second dimension. More importantly, it also provides ^{13}C - ^1H dipolar couplings characteristic of different sub-units of the molecule in the banana phase. These dipolar couplings could be used to estimate the order parameters of the different segments of the molecule from which the bent-angle in the banana phase could be calculated in a straight forward manner.

2. Experimental Section

The compounds, namely 1,3-phenylene bis{4-[4-(4-n-dodecyloxybenzoyloxy)benzylideneamino]benzoate} (DBPPDO) and 1,3-phenylene bis{4-[4-(4-n-dodecylbenzoyloxy)benzylideneamino]benzoate} (DBPPD) were synthesized by multistep synthetic route. The synthetic scheme, experimental protocols and the spectral data are provided in Electronic Supplementary Information (ESI).

Instrumental details

FT-IR spectra of all the compounds were recorded on ABB BOMEM MB3000 spectrometer using KBr pellets. ^1H and ^{13}C NMR spectra in CDCl_3 were recorded on a Bruker AV-III 400 MHz spectrometer at room temperature using tetramethylsilane (TMS) as an internal standard. The resonance frequencies of ^1H and ^{13}C were 400.23 and 100.64 MHz respectively. The texture of the mesophase and the transition temperatures were determined with an Olympus BX50 hot-stage optical polarizing microscope (HOPM) equipped with a Linkam THMS 600 stage with a TMS 94 temperature controller. The photomicrographs were taken using an Olympus C7070 digital camera. Differential scanning calorimetry (DSC) traces were recorded using a DSC Q200 instrument with a heating rate of $10^\circ\text{C}/\text{minute}$ in nitrogen atmosphere. The data obtained from second heating and cooling is used for discussion.

Computational Details

Density functional theory (DFT) has been remarkably successful at providing a means for computing a variety of ground-state properties with an accuracy which rivals that of the post-Hartree-Fock methods. Calculated structures of organic molecules in the ground-state (S_0) with the Becke's three-parameter functional and the

Lee-Yang-Parr functional (B3LYP) functional often provide better agreement with crystal geometries versus other functionals. Thus, the ground state (S_0) geometrical optimization of DBPPD and DBPPDO in gas phase was carried out at the level of B3LYP/6-31G*.^{24,25} The NMR chemical shifts were calculated at B3LYP/6-311+G(2d,p) level of theory using the gauge invariant atomic orbitals (GIAO) method to circumvent the gauge problem using B3LYP/6-31G(d) geometry.²⁶ Cheeseman recommended the 6-311+G(2d,p) basis set for NMR chemical shifts after scrutiny of various basis sets and hence the same was selected for the present study.²⁷ The scale factor determined for B3LYP/6-311+G(2d,p)//B3LYP/6-31G(d) methodology from the previous study was used for the calculation of ^{13}C NMR chemical shifts.²⁸ Accordingly, $d_{\text{scal}} = 0.95d_{\text{calc}} + 0.30$, where d_{calc} and d_{scal} are the calculated and the linearly scaled values of the ^{13}C chemical shifts, respectively. The chemical shift value of tetramethylsilane calculated at the same level of theory was used as the reference (182.5 ppm).²⁸ All calculations were carried out with Gaussian 09 package.²⁹

Polarization Measurements

The polarization measurements of the samples were performed using commercial liquid crystal cells (Instec) with cell gap $5\mu\text{m}$ and electrode area $5\times 5\text{ mm}^2$. The glass plates of the cell were coated with Polyimide for planar alignment of the LC molecules. Polarization studies of both the mesogens were carried out by measuring the voltage drop across a resistance ($1\text{k}\Omega$) connected in series with the sample cell using an oscilloscope (Agilent MSO6012A) by applying triangle voltage from a signal generator (Agilent 33220A) and a high voltage amplifier (Trek 601-2). The temperatures of the samples were regulated using a temperature controller (Instec) equipped with a hot stage.

X-ray measurements

X-Ray diffraction (XRD) studies of the unoriented samples (Lindemann capillary, diameter of 1 mm, Hampton Research, Aliso Viejo, CA, USA) were carried out using PANalytical instrument (DY 1042-Empyrean) operating with a line focused Ni-filtered Cu-K α ($\lambda=1.54 \text{ \AA}$) beam and a linear detector (PIXcel 3D). The sample temperature was controlled with a precision of 0.1°C using a heater and a temperature controller (Linkam).³⁰

Solid state NMR Experiments

Solid state NMR experiments were carried out on a Bruker AV-III 500 MHz NMR spectrometer. All the experiments on a static liquid crystalline sample were performed on a 5mm double resonance probe with a horizontal solenoid coil. The proton and carbon resonance frequencies were 500.17 and 125.79 MHz respectively. The 90° proton pulse width was 4 μ s. For Cross-polarization, a contact time of $\tau = 3 \text{ ms}$ and 62.5 kHz of rf were used in both carbon and proton channels for the Hartmann-Hahn match condition. Proton decoupling during the ¹³C signal acquisition was done by the SPINAL-64³¹ pulse sequence with an rf field strength of 30 kHz. The 1D spectrum was acquired with 512 scans with a recycle delay of 10s to avoid sample heating. For measuring the ¹³C-¹H dipolar couplings of the mesogen in its mesophase, the 2D SLF approach was used and the SAMPI-4 pulse sequence was applied on the oriented sample under static conditions.³² Details of the application of the pulse sequence to liquid crystalline systems have been described elsewhere.^{33,34} The technique gives a 2D spectrum which correlates the proton-carbon dipolar oscillation frequencies along the F₁ dimension on the basis of the carbon chemical shifts along the F₂ dimension. The SAMPI-4 experimental parameters chosen for DBPPD were as follows: Contact

time $\tau = 3\text{ms}$, number of t_1 data points 100, number of t_2 data points 512, number of scans 80, relaxation delay 14 s to minimize sample heating and 90° pulse width $4\mu\text{s}$. A shifted sine bell window function was applied to the time domain data, and the spectrum was processed in the phase sensitive mode.

3. Results and Discussion

The molecules DBPPD and DBPPDO are synthetically novel and hence it will be useful and interesting to study their mesophase behaviour. The strategy adopted for realizing them is shown in Scheme 1(ESI) while their molecular structures are shown in Fig.1 A & B. Both the mesogens are constructed with seven phenyl rings to get the typical banana mesophase. Their terminal chains, however, are different. In DBPPD dodecyl chain is directly linked to the core whereas in DBPPDO the linkage between core and terminal chain is through oxygen. The molecules are symmetric owing to identical side wings. In DBPPDO, insertion of oxygen between core and the terminal chain is likely to influence the mesophase characteristics due to the terminal dipoles and a behavior different from DBPPD may be anticipated. The structural identification of both the mesogens is accomplished by FT-IR in solid phase, by ^1H and ^{13}C NMR spectroscopy in solution. For mesophase characterization, HOPM, DSC and variable temperature powder X-ray diffraction techniques are used. The HOPM investigation revealed the existence of a B_2 phase for DBPPD. The sample upon cooling from the isotropic phase entered a phase where it exhibited a complex texture (Fig.2A) typical of the B_2 phase.³⁵ In this phase, the circular domains in the texture exhibit a brush pattern which are neither parallel nor perpendicular to the polarizers indicating a synclinic organization of the molecules in successive layers. On further cooling, crystallization was noticed. Based on this and on the XRD and polarization measurements discussed below, the B_2 phase is characterized to have a racemic

SmC_sP_A structure. The polarizing optical micrographs of the sample DBPPDO are shown in Fig.2B-D. Interestingly, DBPPDO showed a different behavior and revealed a filamentary texture on cooling the sample from the isotropic phase. Additionally, the HOPM investigation of contact preparations of DBPPD and DBPPDO revealed immiscibility suggesting that the phase of DBPPDO is different from that of DBPPD. From the textures observed in the HOPM studies together with the results of other investigations of the sample reported below, the mesophase has been identified as B₇.³⁶ The appearance of the mesophases enantiotropically for both the mesogens is confirmed by DSC measurements (Fig.3A & B). Table 1 lists phase transition temperatures and the enthalpy values for both the mesogens. The high ΔH values associated with the isotropic to mesophase transition support the banana phase.⁴ A comparison of mesophase transition temperatures of both the mesogens indicate only marginal difference. For instance, DBPPDO exhibits lower melting and clearing temperatures in contrast to DBPPD, but the mesophase range for DBPPDO is slightly higher than DBPPD (1.6 °C). The existence of lamellar ordering in the B₂ and B₇ mesophases is confirmed by variable temperature powder XRD measurements. The molecular shape as well as the length (L) has been arrived at by DFT based quantum chemical calculations of energy minimized structures. For DBPPD, ¹³C NMR studies in the liquid crystalline phase have been carried out and the orientational order parameters and the bent-angle have been obtained.

Electric Polarization Studies

In the B₂ phase of DBPPD, the current through the liquid crystal cell under the application of the triangular wave voltage (36 V, 80 Hz) is shown in Fig.4A. The existence of two current peaks in each half period of the applied voltage indicates the anti-ferroelectric organization of the layer polarizations in successive layers. The

polarization measurements in conjunction with the HOPM studies indicate a racemic SmC_sP_A structure of the B_2 phase of the compound DBPPD. The polarization value of the layers can be determined by measuring the area of the current peaks. The variation of the polarization of the layers with temperature is shown in Fig.4B. In the isotropic phase, the polarization value is zero. As the sample is cooled to the B_2 phase, the value of the polarization increases with decreasing temperature and tends to saturate at lower temperatures. The saturated value of the polarization for DBPPD is found to be 650 nC/cm^2 . For the other mesogen, DBPPDO, the polarization current peaks in the mesophase are not observed even with the application of relatively high voltage ($14 \text{ V}/\mu\text{m}$). This is in conformity with the behavior generally expected of the B_7 mesophase^{3,6-8} and serves as additional evidence for the conclusion arrived at based on the HOPM studies.

Variable Temperature Powder X-ray diffraction studies

For DBPPD, the X-ray measurements are carried out in the temperature range $155\text{-}205^\circ\text{C}$. In the mesophase range, multiple sharp reflection peaks in the small angle region are observed in addition to a diffuse peak in the wide angle region. Table 2 shows the d-values corresponding to the XRD peaks at different temperatures. The XRD intensity versus 2θ plot at 185°C is shown in Fig.5A. The four small angle peaks are in the ratio of 1:2:3:4 of the wave number which confirm the lamellar structure of the mesophase with layer spacing as 44.29 \AA . The diffuse peak in the wide angle region indicates the liquid like correlation of the molecules in the smectic layers and liquid like nature of the terminal chains. The molecular length (L) along the bow-string direction of bent-core molecule obtained from energy optimized structure using DFT calculations is 55.7 \AA . The higher value of L than the layer spacing indicates that the molecules are tilted $\sim 37.3^\circ$ with respect to the layer normal. Thus, the results of the

X-ray diffraction studies are consistent with the identification of the phase in DBPPD as the B₂ mesophase.

The XRD intensity versus 2θ plot of DBPPDO at 175° C is shown in Fig.5B. Table 3 shows the d-values corresponding to the XRD peaks at different temperatures. The two small angle peaks in the ratio of 1:2 of the wave number indicate the lamellar structure of the mesophase with layer spacing as 44.88 Å. The diffuse peak in the wide angle region indicates the liquid like correlation of the molecules in the smectic layers. The molecular length (L) along the bow-string direction of the bent-core molecule obtained from energy optimized structure from DFT is 57.2 Å. From this the tilt angle of the molecules with respect to the layer normal is calculated as 38.3°. Even though the XRD studies indicate a simple lamellar structure for the mesophase, the phase is still assigned as the B₇ phase based on the HOPM and the switching current studies. The absence of a complex XRD pattern expected for the B₇ phase due to layer modulations is possibly the result of the periodicity of layer modulations being large compared to the layer spacing and hence not visible in the XRD pattern. Indeed for many banana molecules, the B₇ phase revealed only lamellar ordering in XRD even though the HOPM textures are consistent with the typical B₇ textures.^{3, 11, 36a, 37, 38} For instance, Pyc et al.³⁸ observed for the B₇ mesophases in resorcinol based mesogens that apart from the main 001 reflection, no additional signals in the X-ray diffraction patterns are noticed. This absence of satellite X-ray signals around the main Bragg (001) reflection has been attributed to a very long undulation period of more than 1000 Å, estimated from the resolution of the apparatus. Further the contact preparations of DBPPD and DBPPDO in HOPM revealed immiscibility suggesting that the phase of DBPPDO is different from that of DBPPD, namely the B₂ phase. Based on these observations, we take the available results of the HOPM, polarization and XRD

measurements as indicative of a B_7 phase in DBPPDO. It is also pertinent to note that from the DFT calculations, the dipole moment of the DBPPDO molecule is found to be 10.0 D which is larger than 5.9 D of DBPPD molecule. This is again supportive of the formation of a B_7 phase in DBPPDO since a larger polarization of the layers is expected to stabilize the B_7 phase.⁷

¹³C NMR studies of DBPPD

Solution phase

The proton decoupled ¹³C NMR spectrum of DBPPD is shown in Fig. 6A. The spectrum shows 19 sharp lines with varying intensities in the range 115-165 ppm. Since the mesogen has C_2 symmetry, only one resonance for every pair of carbons related by symmetry in the central phenyl ring and the side-wings is expected. A close inspection of the spectrum reveals six sharp and intense lines arising from side wing phenyl ring carbons. The CH carbons of central phenyl ring and imine show medium intensity whereas the low intensity signals are assigned to quaternary carbons. The detailed assignment of the spectrum is carried out by comparison with ¹³C NMR chemical shifts computed by the DFT method. Table 4 lists the chemical shift values of all core unit carbons along with assignment. For the terminal dodecyl chain, 11 lines are observed among which the signal from the OCH₂ of the terminal chain is noticed at 36.1 ppm and that of the methyl carbon at 14.2 ppm. The other methylene carbon signals are seen in the range 22-32 ppm. Similar approach has also been followed for assigning the ¹³C spectrum of DBPPDO using DFT results (Table 5).

Banana Phase

It has been generally observed that it is difficult to align molecules in the banana phase in the magnetic field.^{20,21} In the present study, the banana phase of DBPPDO did

not align in magnetic field and hence the NMR spectrum of the aligned sample could not be obtained. On the other hand, DBPPD, in its B₂ phase could be aligned by cooling the sample from the isotropic melt in the magnetic field. Its ¹³C spectrum recorded at 190 °C is shown in Fig.6B. The observation of identifiable spectral lines, though broad in comparison to the lines in solution, indicates that the molecules are aligned in the magnetic field. Further confirmation of the magnetic field alignment is provided by the increase in the chemical shift values of the carbons of the central phenyl ring as well as of the side wing core with the simultaneous decrease in the values for the terminal chain carbons. The chemical shift range for the core carbons in the oriented phase is found to be 132-207 ppm. Due to broadening of the spectral lines and possible overlap, the number of identifiable peaks in the B₂ phase is reduced to 12 from the 19 carbon peaks that are distinguished in the solution spectrum. Thus in the region 132-150 ppm, four peaks are observed with a large intensity. About eight peaks with small intensity can be distinguished in the region 170-207 ppm. For the terminal chain, all the peaks are merged in the range 23-26 ppm except the terminal methyl which is distinguished at 10.6 ppm. The alignment induced chemical shifts suggest that the molecular axis is parallel to the magnetic field. The chemical shift assignment of the static liquid crystalline spectrum, in which many carbon signals are overlapped, is facilitated by the 2D-SLF data where separation of several superimposed signals could be achieved owing to the difference in the magnitude of ¹³C-¹H dipolar couplings of the carbons. The measurement of the dipolar couplings also lead to the estimation of the order parameters of the central and side-wing phenyl rings from which the bent-angle of was determined. These are detailed in the next section.

2D NMR in the B₂ (SmC_SP_A) Phase

Fig.7 shows the 2D-SLF spectrum of DBPPD obtained at 190 °C in B₂ phase. The spectrum shows contours with different intensities arising from the central as well as the side-wing phenyl rings and their linking units. In the region 130-151 ppm, where the 1D spectrum showed 4 intense peaks, the 2D spectrum revealed 7 contours that could be clearly distinguished. Similarly, for the region 174-207 ppm in the 1-D spectrum which showed highly overlapped low intensity peaks, the 2-D spectrum displays well resolved contours by virtue of the difference in the ¹³C-¹H dipolar couplings of the different carbons. Based on the magnitude of these couplings, the different carbons can be categorized as proton-attached and quaternary carbons. Their location in the molecule and the local molecular order can also be estimated. A particularly important feature of the spectrum is the three well separated contours that appear along the dipolar coupling axis in the range 9.7-12.3 kHz. These large couplings, easily identified with the three distinct non-equivalent carbons at position 17, 18 and 19 in the central phenyl ring, provide crucial information on the assignment of the spectrum and also on the orientation of the mesogen. The methine carbons of the side-wing phenyl rings as well as the azomethine carbon show contours in the range 2-3 kHz while the quaternary carbons of the phenyl ring as well as of the linking units have peaks in the range 0.9-1.6 kHz. The assignment of the carbons and their dipolar frequencies are listed in Table 4. The large difference in the dipolar couplings of the central phenyl ring versus the side -wing phenyl rings provide information of the local order parameters and also a clue on how these different units are oriented with respect to the molecular axis.^{20,39-42} In studies carried out by us recently, a mesogen that mimics the side of arm of a banana molecule and a banana mesogen (PMBAPH) that exhibits a B₁ mesophase^{43,44} have also been observed to reveal such

characteristic dipolar couplings leading to the estimation of the orientational order parameters and the molecular topology. The ^{13}C - ^1H dipolar couplings are related to the local orientational order parameters of the phenyl rings which can be calculated using the following equation^{20a,33,45}

$$D_{C-H} = K \left\{ \frac{1}{2} (3 \cos^2 \theta_z - 1) S'_{zz} + \frac{1}{2} (\cos^2 \theta_x - \cos^2 \theta_y) (S'_{xx} - S'_{yy}) \right\} \quad (1)$$

where $K = -h\gamma_H\gamma_C/4\pi^2 r_{CH}^3$, with γ_H and γ_C are the gyromagnetic ratios of protons and carbons respectively, r_{CH} is the distance between the proton and carbon nuclei and θ_x , θ_y and θ_z are angles between r_{CH} dipolar vector and the coordinate axes. Standard bond distances, namely 1.1 Å for the C–H bond and 1.4 Å for the C–C bond, are taken for calculating K in equation (1). For the side-wing phenyl rings, the para axis of the ring is taken as z' -axis while x' -axis is the in-plane axis perpendicular to z' . For the central phenyl ring we have taken the line passing through carbons 18 and 19 as the x -axis while the axis perpendicular to it and in the plane of the ring as the major ordering axis (z -axis). This is in accordance with the high ^{13}C - ^1H dipolar couplings noticed for the central phenyl rings. From the experimental dipolar oscillation frequencies (Table 4) obtained from the SAMPI-4 experiment, the dipolar couplings can be extracted in the following manner. In the case of side arm phenyl rings, methine carbon experimental dipolar frequency has two coupling components, namely, a coupling between attached *ipso* proton D_{C-Hi} and also a coupling to its non-bonded *ortho* proton D_{C-Ho} . Hence, the final frequency will be $[(D_{C-Hi})^2 + (D_{C-Ho})^2]^{1/2}$.⁴¹ For the quaternary carbon coupled to two equivalent *ortho* protons, the dipolar frequency is given by $\sqrt{2} \cdot (D_{C-Ho})$. For the central phenyl ring, the experimentally measured dipolar frequency for the C17 carbon can be expressed as $[(D_{C17-H17})^2 + (D_{C17-H18})^2]^{1/2}$ and for the C18 carbon the dipolar frequency is given by $[(D_{C18-H18})^2 + 2(D_{C18-H17})^2]^{1/2}$. For the C19 carbon we considered coupling only to its attached proton i.e., $(D_{C19-H19})$. For

obtaining the best fit of equation (1) to the experimental values, it has been found necessary, in the case of side-wing phenyl rings, to slightly vary the two CCH bond angles around the ideal hexagonal geometry of 120° .^{42a} Similarly, for the central phenyl ring, the angles made by $C_{18}-H_{18}$ and $C_{19}-H_{19}$ bonds with respect to the local z -axis have been equally varied around 90° to retain the symmetry of the ring. So also the angle between $C_{17}-H_{17}$ bond and z -axis has been varied around 30° to arrive at the best fit. The calculated order parameters for the side-wing and central phenyl rings are listed in Table 6. From the Table 6, it may be noticed that for all the side-wing phenyl rings S'_{zz} is the same equal to 0.53. The biaxial order parameter ($S'_{xx} - S'_{yy}$) is also nearly same and small by an order of magnitude compared to S'_{zz} . This can be taken to indicate that the long molecular axis for the side-wing is essentially parallel to the para axes of the wing phenyl rings. The central phenyl ring also shows essentially a single order parameter but with a value of 0.84 that is significantly large compared to the side-wing phenyl rings. Based on the earlier studies, this is also the order parameter of the orienting axis of the molecule.^{17, 20, 21, 44} From the values of the order parameters of the side-wing phenyl rings (S^w_{zz}) and the central ring (S^c_{zz}), the angle β (Fig.8) the side-wings make with the orienting axis of the molecule can be calculated from $S^w_{zz} \approx S^c_{zz} P_2(\cos\beta)$.^{39a,c} For the present case β is found to be 29.7° and hence the bent-angle between the two side wings of DBPPD is 120.5° . This value of the bent-angle is in good agreement with those reported in literature.^{17, 20, 21}

The ^{13}C NMR spectra of DBPPD were also recorded at a few other temperatures in the range $160\text{-}208^\circ\text{C}$. Unlike calamitic mesogens, DBPPD did not show significant variation in the chemical shift values with change in temperature. For instance, the methine carbons of side-wing phenyl rings exhibited a variation of $1\text{-}1.6$ ppm in the temperature range while the central phenyl ring showed more or less the same

chemical shifts. The small variation in chemical shifts with change in temperature suggests that the order parameter is most likely temperature independent. These results are on expected lines for the banana liquid crystals and in agreement with observations made earlier on other systems.^{1,17,21} It may be mentioned here that in some of the earlier studies of the banana mesogens, the bent-angles have been determined from ^{13}C chemical shifts in the mesophase using 1D ^{13}C NMR spectra.¹⁷ This approach requires identifying relevant resonances in the spectrum and assigning them to the individual carbons. Due to the large line-widths encountered in the case of the banana mesogens, this sometimes is a major challenge.^{17b} The 2D approach employed here on the one hand mitigates this problem by providing increased resolution in the second dimension and on the other hand provides the ^{13}C - ^1H dipolar couplings which provide a simple and straightforward means of estimating the order parameter values. As sufficient data on banana mesogens is accumulated over time, it is anticipated that a visual examination of the 2D spectrum would reveal the nature of the orientation of the different structural units. The other highlights of the present study are that the molecules investigated are synthetically novel. Despite a common core, they reveal different phases for the dodecyl homolog and the dodecyloxy homolog which are attributable to a large difference in their dipole moments. The dodecyloxy homolog did not orient in the magnetic field whereas magnetic field orientation has been achieved for the other, leading to useful information about the mesogen. Thus a slight change in the terminal unit is observed to result in a dramatic change in the mesophase characteristics.

4. Conclusion

The structural investigations of two banana mesogens based on resorcinol with terminal alkyl/alkoxy chains revealed some interesting features. Both the mesogens

exhibited banana mesophases as revealed by HOPM, DSC, XRD and polarization measurements. The difference in the mesophase range of synthesized mesogens was found to be very marginal while phase structures were dramatically different. The dodecyl homolog exhibited the SmC_SP_A phase whereas the dodecyloxy analog showed B_7 mesophase. The XRD measurements support layer ordering for both the mesogens. The appearance of the B_7 for dodecyloxy homolog was attributed to its high dipole moment (10.0 D) in contrast to dodecyl homolog (5.9 D). Thus, the terminal dipoles seem to largely influence the phase change for dodecyloxy homolog. The ^{13}C NMR studies of dodecyl homolog provide orientational order parameter values from which the bent-angle is calculated to be 120.5° which is yet another characteristic feature of banana mesogens. The 2D NMR approach presented here is expected to be a convenient means of characterizing the banana mesophases in view of the enhanced resolution and the availability of dipolar couplings along with chemical shifts as an additional source of structural and dynamics information.

Electronic Supplementary Information (ESI) available: It contains Synthetic details and figure of SAMPI-4 dipolar cross-sections. See DOI: 10.1039/b000000x

Acknowledgments

M. K. R would like to thank Prof. K. Subramanyam Reddy, Sri Venkateswara University, Tirupati, India and Dr. A. B. Mandal, Director, CSIR-CLRI, Chennai, India for their help, encouragement and support. The authors are thankful to Dr. V. Subramanian, CLRI, for the quantum chemical calculations. M. K. R and T. N. S are grateful to Prof. V. A. Raghunathan and Ms. K. N. Vasudha, Raman Research Institute, Bangalore, India for the X-ray measurements and to Dr. R. Amaranatha Reddy, Sr. Research Chemist at PPG Industries

Inc, USA, for technical discussions. TNS also acknowledges the partial financial support from STRAIT project under XII five year plan of CSIR. The use of the NMR spectrometers namely, Bruker AV-III 400 MHz solution state and Bruker AV-III-500 MHz solid state funded by the Department of Science and Technology, New Delhi, at the NMR Research Centre, Indian Institute of Science, Bangalore, India is gratefully acknowledged.

[‡]*Department of Chemistry, S.V.University, Tirupati 517502, India. E-mail: kesavareddy2000@gmail.com*

[†]*Chemical Laboratory and Polymer Laboratory, CSIR-Central Leather Research Institute, Adyar, Chennai 600020, India. E-mails: varathan.elumalai85@gmail.com and tnswamy99@hotmail.com*

[#]*Soft Condensed Matter, Raman Research Institute, Bangalore, India. E-mails: bjacintha01@gmail.com and aroy@rri.res.in*

[§]*Department of Physics, Indian Institute of Science, Bangalore 560012, India. E-mail: nitinlobo@gmail.com*

[♦]*NMR Research Centre, Indian Institute of Science, Bangalore 560012, India. E-mail: kvr@sif.iisc.ernet.in*

^a*Current address: Chemical Physics Laboratory, CSIR-Central Leather Research Institute, Adyar, Chennai 600020, India.*

REFERENCES

1. G. Pelzl, S. Diele and W. Weissflog, *Adv. Mater.*, 1999, **11**, 707-724.
2. M. B. Ros, J. L. Serrano, M. Rosario de la Fuente and C. L. Folcia, *J. Mater. Chem.*, 2005, **15**, 5093-5098.
3. H. Takezoe and Y. Takanishi, *Jpn. J. Appl. Phys.*, 2006, **45**, 597-625.
4. R. Amaranatha Reddy and C. Tschierske, *J. Mater. Chem.*, 2006, **16**, 907-961.
5. A. Eremin and A. Jakli, *Soft Matter*, 2013, **9**, 615-637.
6. N. Vaupotic, D. Pocięcha and E. Gorecka, *Top. Curr. Chem.*, 2012, **318**, 281-302.
7. (a) D. R. Link, G. Natale, R. Shao, J. E. MacLennan, N. A. Clark, E. Korblova and D. M. Walba, *Science*, 1997, **278**, 1924-1927. (b) D. A. Coleman, J. Fernsler, N. Chattham, M. Nakata, Y. Takanishi, E. Korblova, D. R. Link, R.-F. Shao, W. G. Jang, J. E. MacLennan, O. Mondainn-Monval, C. Boyer, W. Weissflog, G. Pelzl, L.-C. Chien, J. Zasadzinski, J. Watanabe, D. M. Walba, H. Takezoe and N. A. Clark, *Science*, 2003, **301**, 1204-1211.
8. (a) R. Amaranatha Reddy, U. Baumeister, C. Keith and C. Tschierske, *J. Mater. Chem.*, 2007, **17**, 62-75. (b) R. Amaranatha Reddy, C. Zhu, R. Shao, E. Korblova, T. Gong, Y. Shen, E. Garcia, M. A. Glaser, J. E. MacLennan, D. M. Walba and N. A. Clark, *Science*, 2011, **332**, 72-77.
9. M. Hird, *Liquid Crystals Today*, 2005, **14**, 9-21.
10. J. Etxebarria and M. Blanca Ros, *J. Mater. Chem.*, 2008, **18**, 2919-2926.
11. W. Weissflog, H. Nadasi, U. Dunemann, G. Pelzl, S. Diele, A. Eremin and H. Kresse, *J. Mater. Chem.*, 2001, **11**, 2748-2758.
12. W. Weissflog, H. N. Shreenivasa Murthy, S. Diele and G. Pelzl, *Phil. Trans. R. Soc. A*, 2006, **364**, 2657-2679.
13. R. Amaranatha Reddy and B. K. Sadashiva, *J. Mater. Chem.*, 2004, **14**, 310-319.

14. R. Amaranatha Reddy and B. K. Sadashiva, *J. Mater. Chem.*, 2002, **12**, 2627-2632.
15. M. Kohout, J. Tuma, J. Svoboda, V. Novotna, E. Gorecka and D. Pocięcha, *J. Mater. Chem. C*, 2013, **1**, 4962-4969.
16. S. Kang, R. Ishige, E.-W. Lee, M. Tokita and J. Watanabe, *J. Mater. Chem.*, 2012, **22**, 21448-21452.
17. (a) A. Eremin, H. Nádasi, G. Pelzl, S. Diele, H. Kresse, W. Weissflog and S. Grande, *Phys. Chem. Chem. Phys.*, 2004, **6**, 1290-1298. (b) W. Weissflog, U. Dunemann, M. W. Schroder, S. Diele, G. Pelzl, H. Kresse and S. Grande, *J. Mater. Chem.*, 2005, **15**, 939-946. (c) I. Wirth, S. Diele, A. Eremin, G. Pelzl, S. Grande, L. Kovalenko, N. Pancenko and W. Weissflog, *J. Mater. Chem.*, 2001, **11**, 1642-1650. (d) H. Nádasi, W. Weissflog, A. Eremin, G. Pelzl, S. Diele, B. Das and S. Grande, *J. Mater. Chem.*, 2002, **12**, 1316-1324.
18. K. Yamada, S. Kang, K. Takimoto, M. Hattori, K. Shirata, S. Kawauchi, K. Deguchi, T. Shimizu and J. Watanabe, *J. Phys. Chem. B*, 2013, **117**, 6830-6838.
19. D. M. Walba, L. Eshdat, E. Korblova and R.K. Shoemaker, *Cryst. Growth Des.*, 2005, **5**, 2091-2099.
20. (a) J. Xu, K. Fodor-Csorba and R. Y. Dong, *J. Phys. Chem. A*, 2005, **109**, 1998-2005. (b) R.Y Dong, *J. Phys. Chem. B*, 2009, **113**, 1933-1939. (c) J. Xu, R. Y. Dong, V. Domenici, K. Fodor-Csorba and C. A. Veracini, *J. Phys. Chem. B*, 2006, **110**, 9434-9441.
21. (a) V. Domenici, C. A. Veracini and B. Zalar, *Soft Matter*, 2005, **1**, 408-411. (b) V. Domenici, *Soft Matter*, 2011, **7**, 1589-1598. (c) R.Y. Dong, K. Fodor-Csorba, J. Xu, V. Domenici, G. Prampolini and C. A. Veracini, *J. Phys. Chem. B*, 2004, **108**, 7694-7701. (d) V. Domenici, C. A. Veracini, K. Fodor-Csorba, G. Prampolini, I. Cacelli, A. Lebar and B. Zalar, *ChemPhysChem.*, 2007, **8**, 2321-2330.
22. L. Rahman, Sandeep Kumar, C. Tschierske, G. Israel, D. Ster and G.Hegde, *Liq. Cryst.*, 2009, **36**, 397-407.
23. M. Alaasar, M. Prehm and C. Tschierske, *Liq. Cryst.*, 2013, **40**, 656-668.
24. A. D. Becke, *J. Chem. Phys.*, 1993, **98**, 5648-5652.

25. C.T. Lee, W. T. Yang and R. G. Parr, *Phys. Rev. B*, 1988, **37**, 785-789.
26. R. Ditchfield, *J. Chem. Phys.*, 1972, **56**, 5688-5691.
27. J. R. Cheeseman, G. W. Trucks, T. A. Keith and M. J. Frisch, *J. Chem. Phys.*, 1996, **104**, 5497-5509.
28. A. E. Aliev, D. C. Murias and S. Zhou, *J. Mol. Struct.: Theochem.*, 2009, **893**, 1-5.
29. M. J. Frisch, G. W. Trucks, H. B. Schlegel, G. E. Scuseria, M. A. Robb, J. R. Cheeseman, G. Scalmani, V. Barone, B. Mennucci and G. A. Petersson et al. GAUSSIAN 09, Revision A.02; Gaussian, Inc.: Wallingford, CT, 2009.
30. S. K. Gupta, S. Setia, S. Sidiq, M. Gupta, S. Kumar and S. K. Pal, *RSC Adv.*, 2013, **3**, 12060-12065.
31. B. M. Fung, A. K. Khitrin and K. Ermolaev, *J. Magn. Reson.*, 2000, **142**, 97-101.
32. A. A. Nevzorov and S. J. Opella, *J. Magn. Reson.*, 2007, **185**, 59-70.
33. (a) S. Kalaivani, T. Narasimhaswamy, B. B. Das, N. P. Lobo and K. V. Ramanathan, *J. Phys. Chem. B*, 2011, **115**, 11554-11565. (b) M. Kesava Reddy, K. Subramanyam Reddy, K. Yoga, M. Prakash, T. Narasimhaswamy, A. B. Mandal, N. P. Lobo, K. V. Ramanathan, D. S. Shankar Rao and S. Krishna Prasad, *J. Phys. Chem. B*, 2013, **117**, 5718-5729. (c) M. Kesava Reddy, K. Subramanyam Reddy, T. Narasimhaswamy, B. B. Das, N. P. Lobo and K. V. Ramanathan, *New J. Chem.*, 2013, **37**, 3195-3206.
34. B. B. Das, T. G. Ajitkumar and K. V. Ramanathan, *Solid State NMR.*, 2008, **33**, 57-63.
35. I. Dierking, *Textures of Liquid Crystals*, Wiley-VCH Verlag GmbH, Weinheim, 2003.
36. (a) R. Amaranatha Reddy and B. K. Sadashiva, *Liq. Cryst.*, 2003, **30**, 273-283. (b) D. S. Shankar Rao, Geetha G. Nair, S. Krishna Prasad, S. Anita Nagamani and C. V. Yelamaggad, *Liq. Cryst.*, 2001, **28**, 1239-1243.
37. G. Pelzl, M.G. Tamba, S. Findeisen-Tandel, M.W. Schroder, U. Baumeister, S. Diele and W. Weissflog, *J. Mater. Chem.*, 2008, **18**, 3017-3031.

38. P. Pyc, J. Mieczkowski, D. Pocięcha, E. Gorecka, B. Donnio and D. Guillon, *J. Mater. Chem.*, 2004, **14**, 2374-2379.
39. (a) R. Y. Dong, *Nuclear Magnetic Resonance of Liquid Crystals*; Springer: New York, 1994. (b) A. Ramamoorthy, Ed. *Thermotropic Liquid Crystals: Recent Advances*; Springer: Dordrecht, The Netherlands, 2007; p 38. (c) V. Domenici, M. Geppi and C. A. Veracini, *Prog. Nucl. Magn. Reson. Spectrosc.*, 2007, **50**, 1-50.
40. (a) J. Courtieu, J. P. Bayle and B. M. Fung, *Prog. Nucl. Magn. Reson. Spectrosc.*, 1994, **26**, 141-169. (b) S. Caldarelli, M. Hong, L. Emsley and A. Pines, *J. Phys. Chem.*, 1996, **100**, 18696-18701.
41. (a) C. S. Nagaraja and K. V. Ramanathan, *Liq. Cryst.*, 1999, **26**, 17-21. (b) Z. Gan, *J. Magn. Reson.*, 2000, **143**, 136-143.
42. (a) B. M. Fung, J. Afzal, T. L. Foss and M.-H. Chau, *J. Chem. Phys.*, 1986, **85**, 4808-4814. (b) H. Dehne, M. Potter, S. Sokolowski, W. Weissflog, S. Diele, G. Pelzl, I. Wirth, H. Kresse, H. Schmalfuss and S. Grande, *Liq. Cryst.*, 2001, **28**, 1269-1277.
43. N. P. Lobo, B. B. Das, T. Narasimhaswamy and K.V. Ramanathan, *RSC Adv.*, 2014, **4**, 33383-33390.
44. M. Kesava Reddy, E. Varathan, N. P. Lobo, B. B. Das, T. Narasimhaswamy, and K. V. Ramanathan, *J. Phys. Chem. C*, 2014, **118**, 15044-15053.
45. (a) B. M. Fung, *Prog. Nucl. Magn. Reson. Spectrosc.*, 2002, **41**, 171-186. (b) B. M. Fung, *Encyclopedia of Magnetic Resonance*, 1996, **4**, 2744-2751.

Table 1: Transition temperatures and enthalpy values of DBPPD and DBPPDO

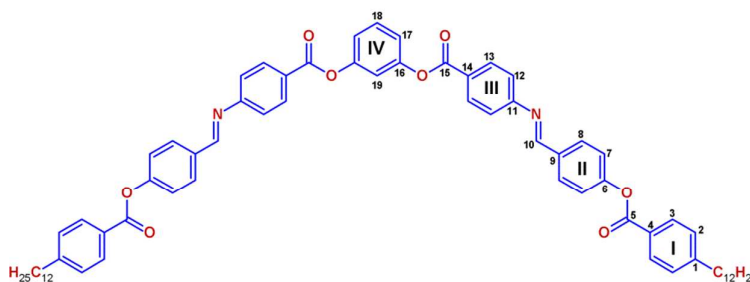
Code	Transition	Temperature (°C)	ΔH (k.cal/mole)	Mesophase range (°C)
DBPPD	Cr-B ₂	157.7	10.31	52.8
	B ₂ -I	210.5	5.47	-
DBPPDO	Cr ₁ -Cr ₂	141.6	4.25	-
	Cr ₂ -B ₇	151.6	4.0	54.4
	B ₇ -I	206.0	4.29	-

Table 2: Powder X-ray diffraction data of DBPPD

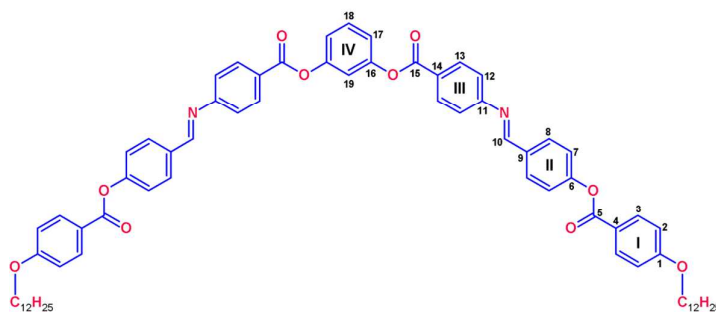
Temperature (°C)	d ₁ (Å)	d ₂ (Å)	d ₃ (Å)	d ₄ (Å)	d ₅ (Å)
205	44.29	22.13	14.88	11.08	4.58
195	44.29	22.13	14.88	11.08	4.57
185	44.29	22.13	14.88	11.08	4.60
175	44.29	22.27	14.88	11.08	4.59
165	44.86	22.27	14.88	11.13	4.59

Table 3: Powder X-ray diffraction data of DBPPDO

Temperature (°C)	d ₁ (Å)	d ₂ (Å)	d ₃ (Å)
200	44.88	22.27	4.60
195	44.88	22.28	4.62
185	44.88	22.77	4.58
175	44.88	22.27	4.52
165	44.88	22.42	4.54
155	44.88	22.42	4.53
145	44.88	22.42	4.54

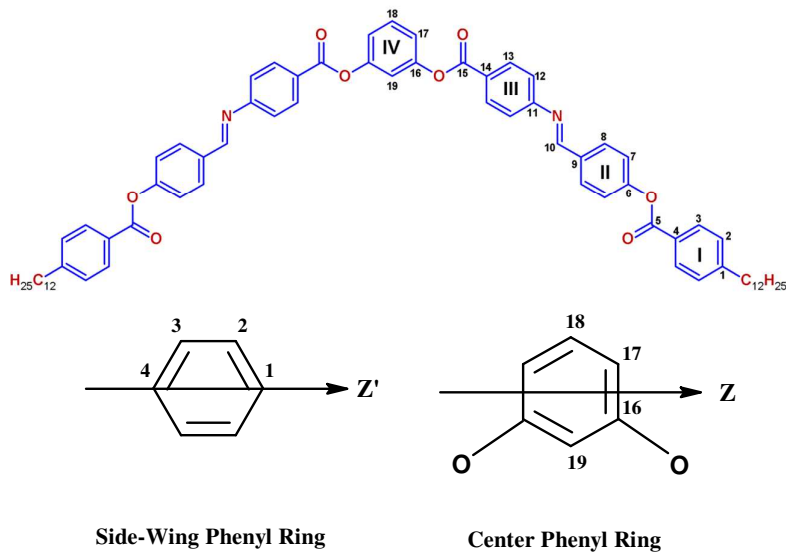
Table 4: ^{13}C NMR data of DBPPD in solution and B_2 phase

C. No	Solution (ppm)	DFT (ppm)	B_2 phase 190 °C (ppm)	Alignment Induced Chemical Shifts (ppm)	^{13}C - ^1H Dipolar Oscillation Frequencies (kHz)
1	149.8	152.7	197.3	47.5	1.32
2	128.7	127.2	145.8	17.1	2.06
3	130.4	128.0	151.9	20.5	2.21
4	126.4	123.4	174.5	48.1	1.14
5	164.8	163.6	191.1	26.3	0.80
6	156.9	156.8	206.6	49.7	1.16
7	122.4	122.2	141.3	18.9	2.16
8	131.6	133.6	150.9	19.3	2.21
9	133.4	132.9	184.7	51.3	1.66
10	160.7	157.7	191.1	30.4	2.99
11	153.9	156.8	202.7	48.8	1.29
12	120.9	124.4	133.1	12.2	2.59
13	130.3	129.0	149.6	19.3	2.52
14	126.6	124.9	174.5	47.9	1.14
15	164.5	162.3	191.1	26.6	0.90
16	151.5	151.9	197.3	45.8	1.31
17	119.2	118.9	178.9	59.7	12.30
18	129.8	126.7	145.8	16.0	10.40
19	115.9	111.7	132.0	16.1	9.70

Table 5: ^{13}C Chemical shifts and DFT values of DBPPDO

Carbon Number	Experimental ^{13}C Chemical shifts (ppm)	DFT (ppm)
1	163.8	164.2
2	114.4	115.5
3	132.4	135.0
4	121.1	117.5
5	164.5	160.2
6	156.9	156.1
7	122.4	122.8
8	131.6	133.4
9	133.3	134.0
10	160.7	157.6
11	154.1	157.0
12	120.9	125.4
13	130.4	129.5
14	129.8	125.6
15	164.5	161.8
16	151.6	152.4
17	119.2	118.2
18	126.5	127.0
19	115.9	110.8

Table 6: Orientational order parameters of DBPPD at 190 °C



Ring	Angles		S'_{zz}	$S'_{xx} - S'_{yy}$
	θ_2	θ_3		
I	120.8	120.1	0.53	0.051
II	120.1	120.3	0.53	0.052
III	119.0	119.1	0.53	0.058
Ring	θ_{18}, θ_{19}	θ_{17}	S_{zz}	$S_{xx} - S_{yy}$
IV	87.5	29.1	0.84	0.024

Figure Captions:

Fig.1: Molecular structures, energy optimized space filled models, magnitude and direction of dipole moment (DFT) of (A) DBPPD and (B) DBPPDO.

Fig.2: HOPM photographs of DBPPD on cooling from isotropic to B₂ phase (A):160.0 °C and DBPPDO: B₇ phase: (B):192.2 °C, (C):188.1 °C, (D):184.2 °C.

Fig.3: DSC scans of (A) DBPPD and (B) DBPPDO.

Fig.4: (A) Current response and the applied triangular wave voltage in the B₂ phase of DBPPD. Two current peaks in each half period of the applied voltage indicate Anti-ferroelectric nature of the sample. (B) Variation of the measured spontaneous polarization in the B₂ phase of DBPPD with temperature.

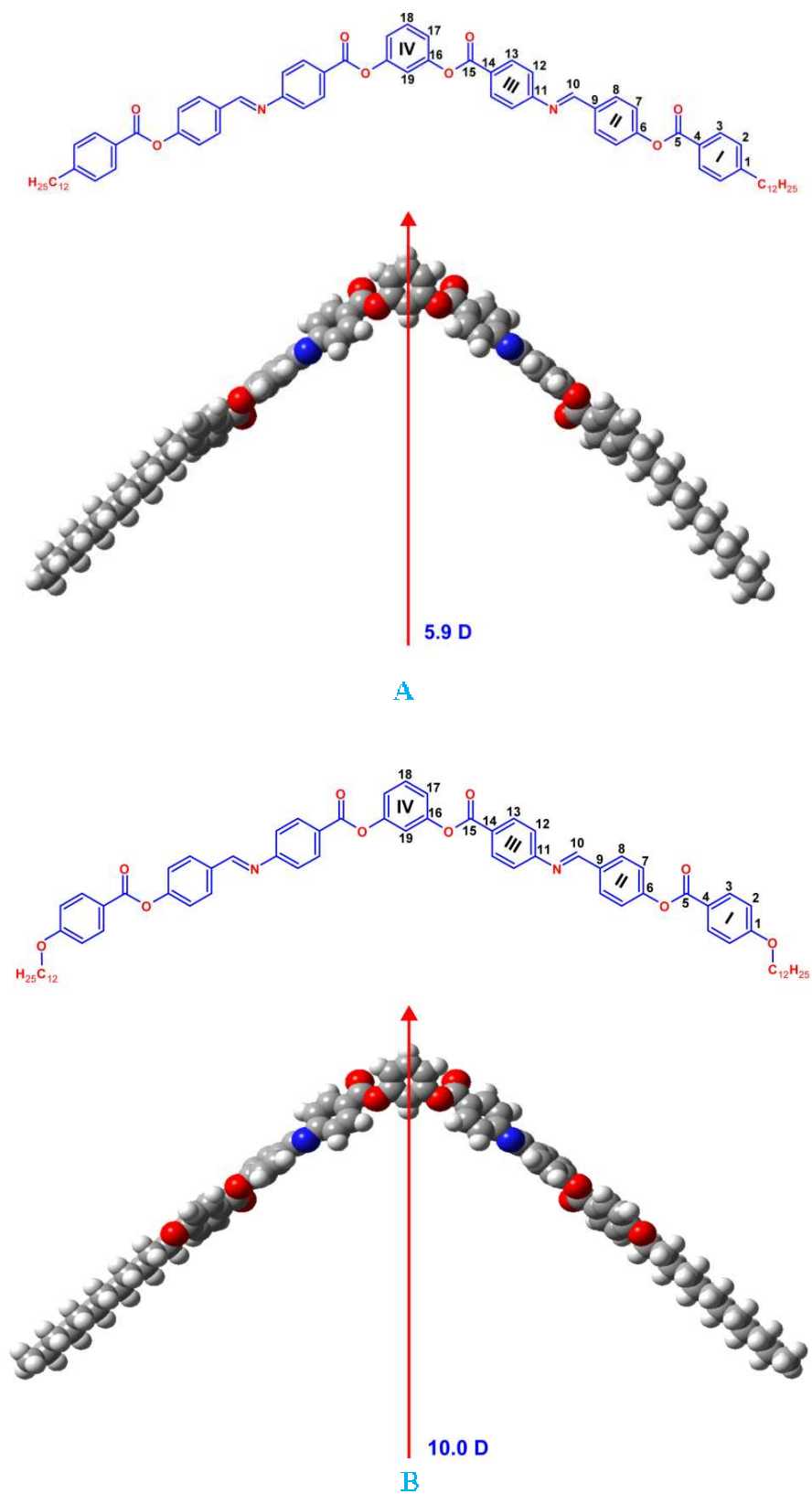
Fig.5: High-resolution X-ray powder diffraction patterns for DBPPD at (A): 185 °C and DBPPDO at (B): 175 °C.

Fig.6: ¹³C NMR spectra of DBPPD in (A) solution and (B) B₂ phase at 190 °C.

Fig.7: 2D SAMPI-4 spectrum of DBPPD in B₂ phase at 190 °C – red contours denote central phenyl ring methine carbons.

Fig.8: Model depicting the molecular frame of DBPPD.

Figure 1



Kesava Reddy et al

Figure 2

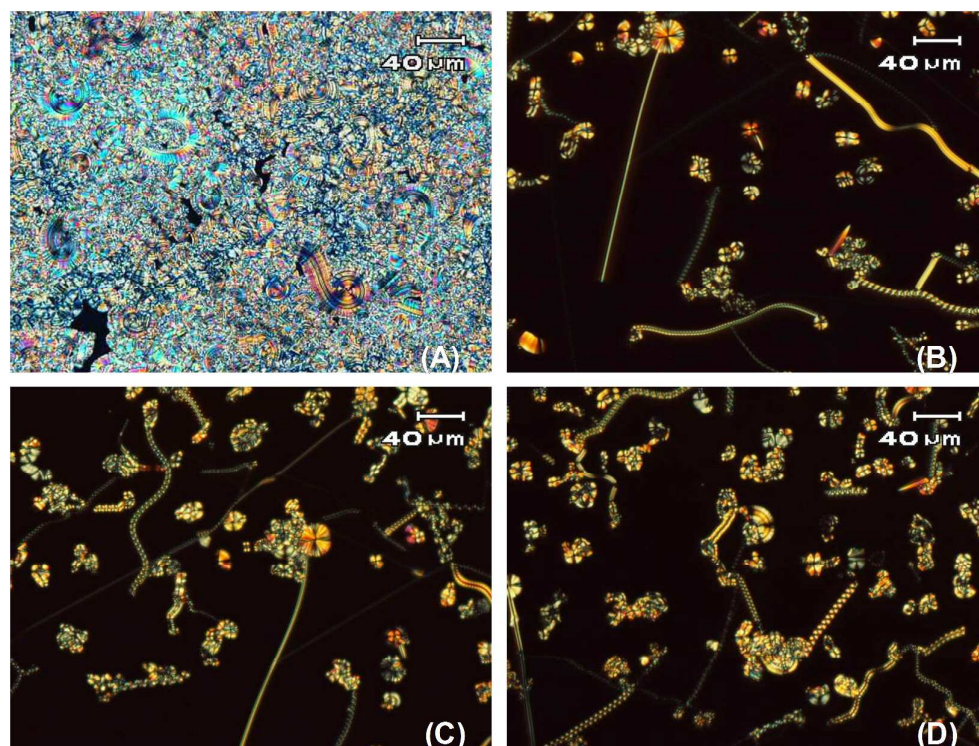
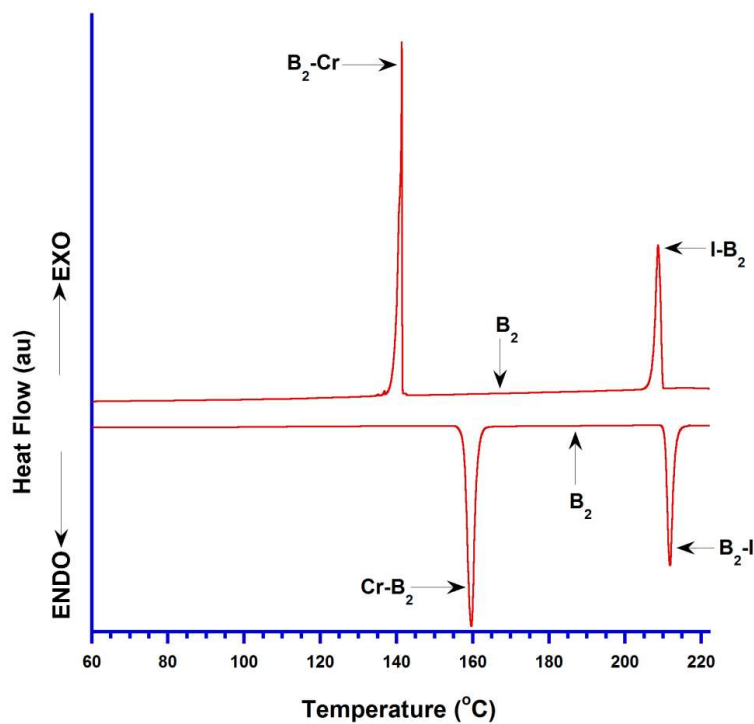
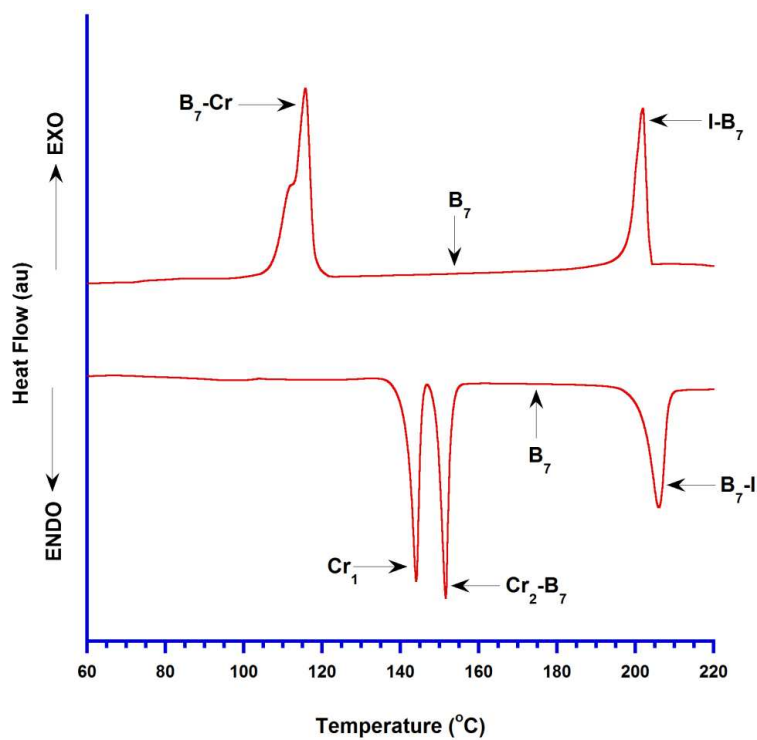


Figure 3

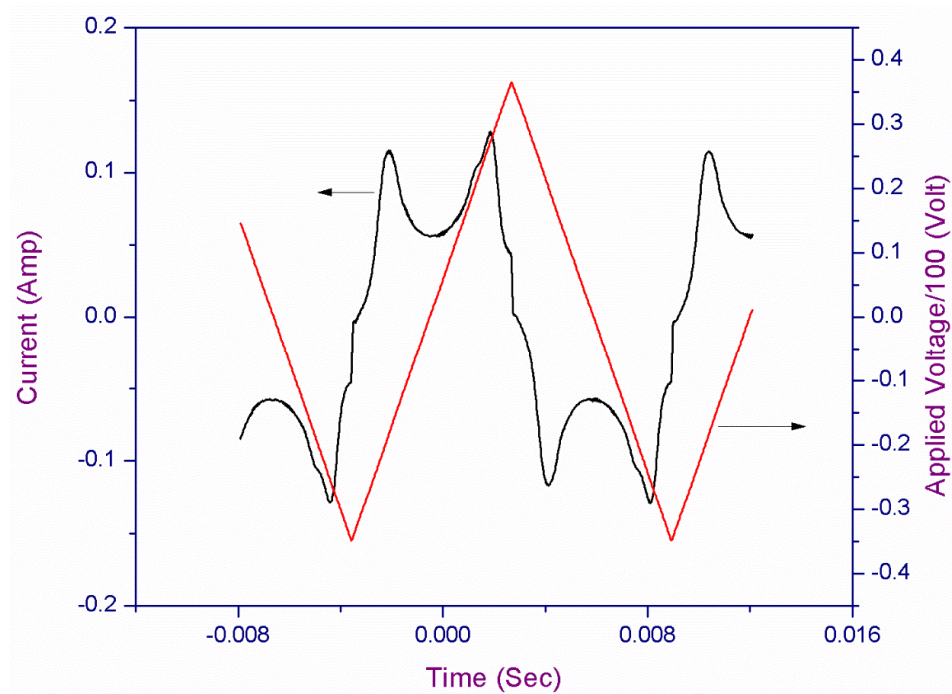


A

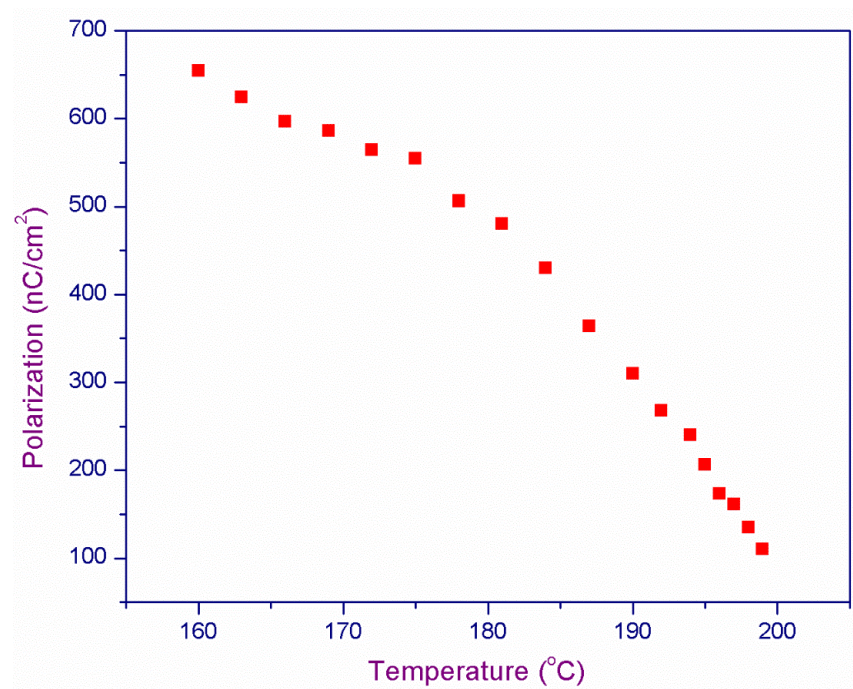


B

Figure 4



A



B

Figure 5

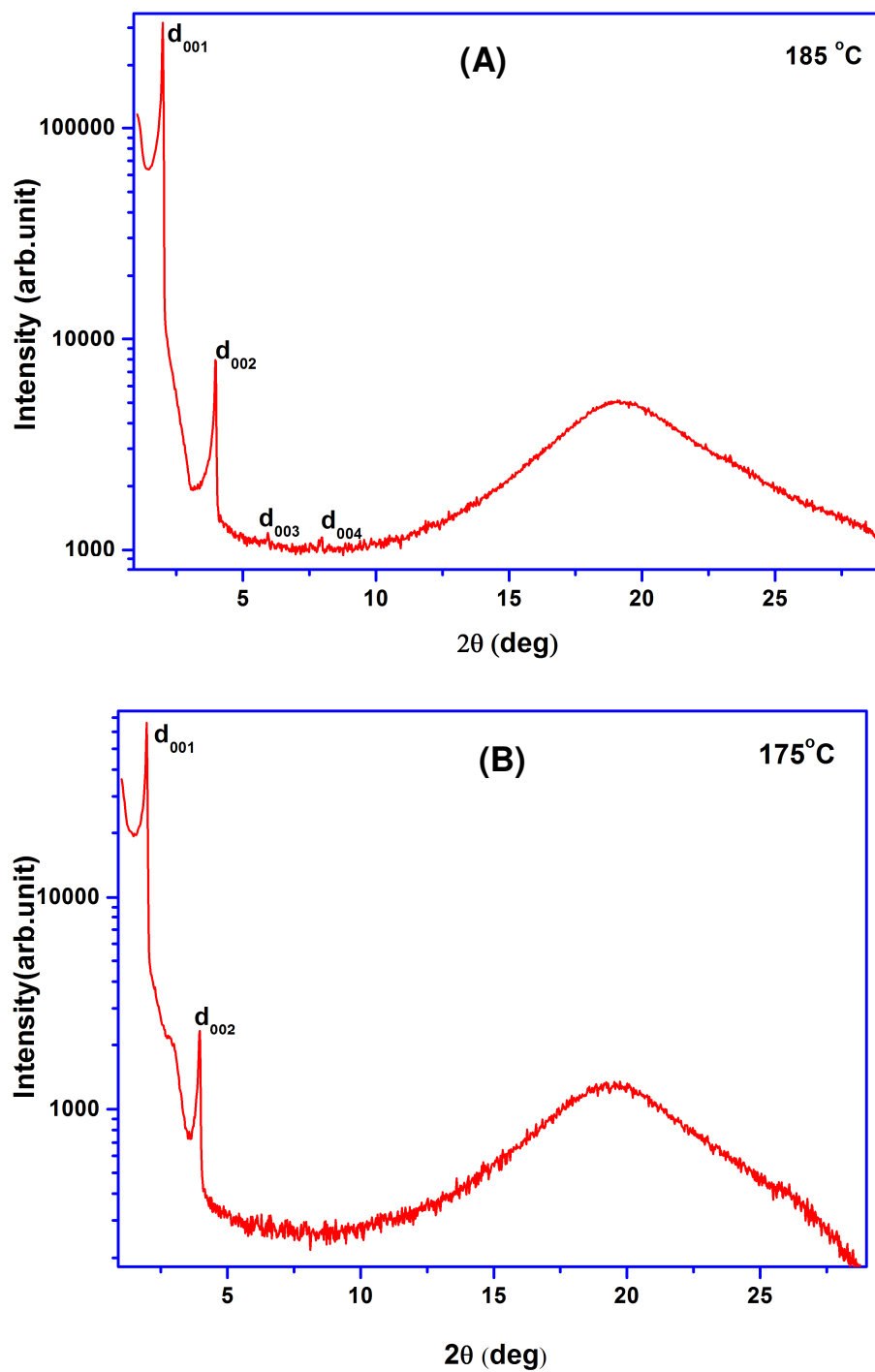


Figure 6

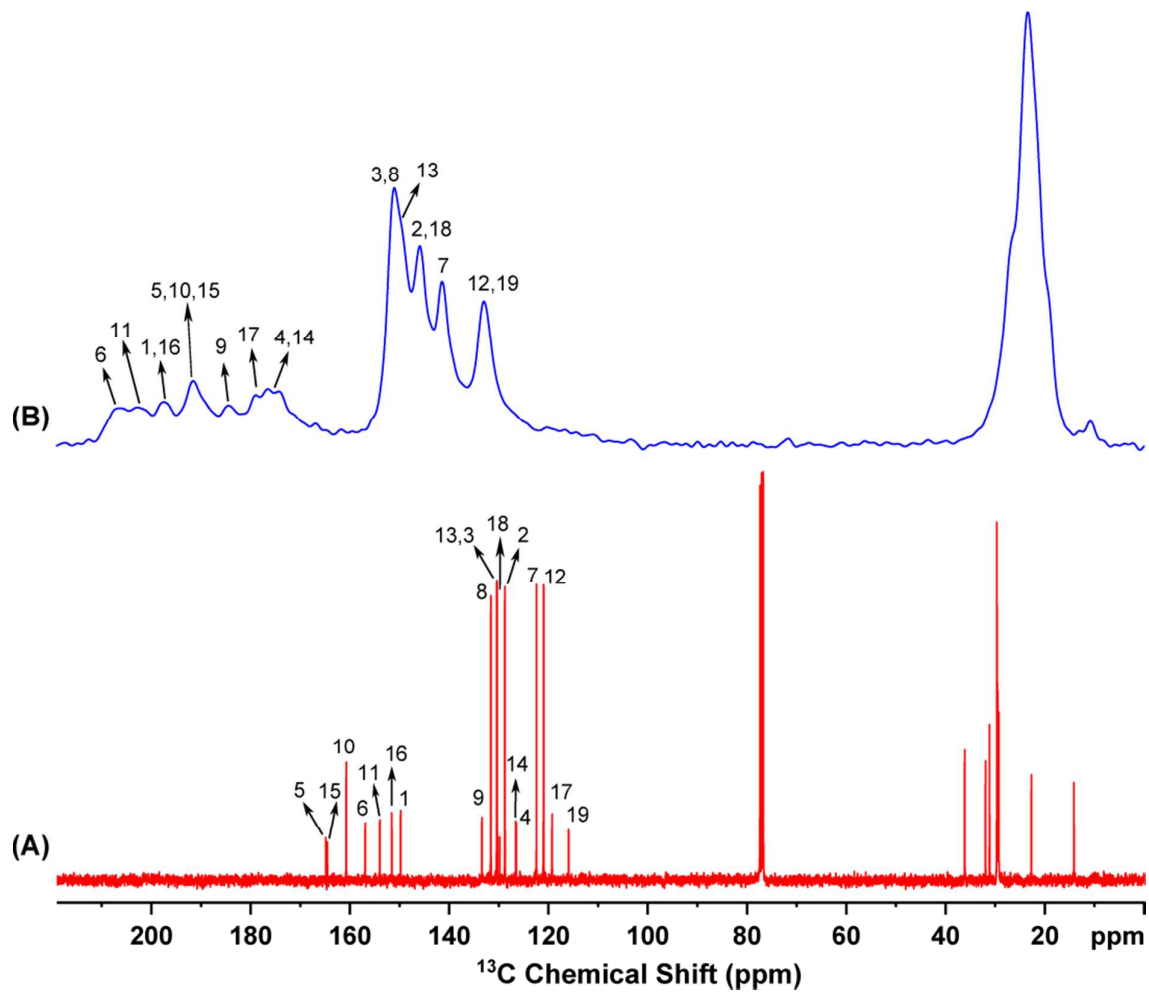
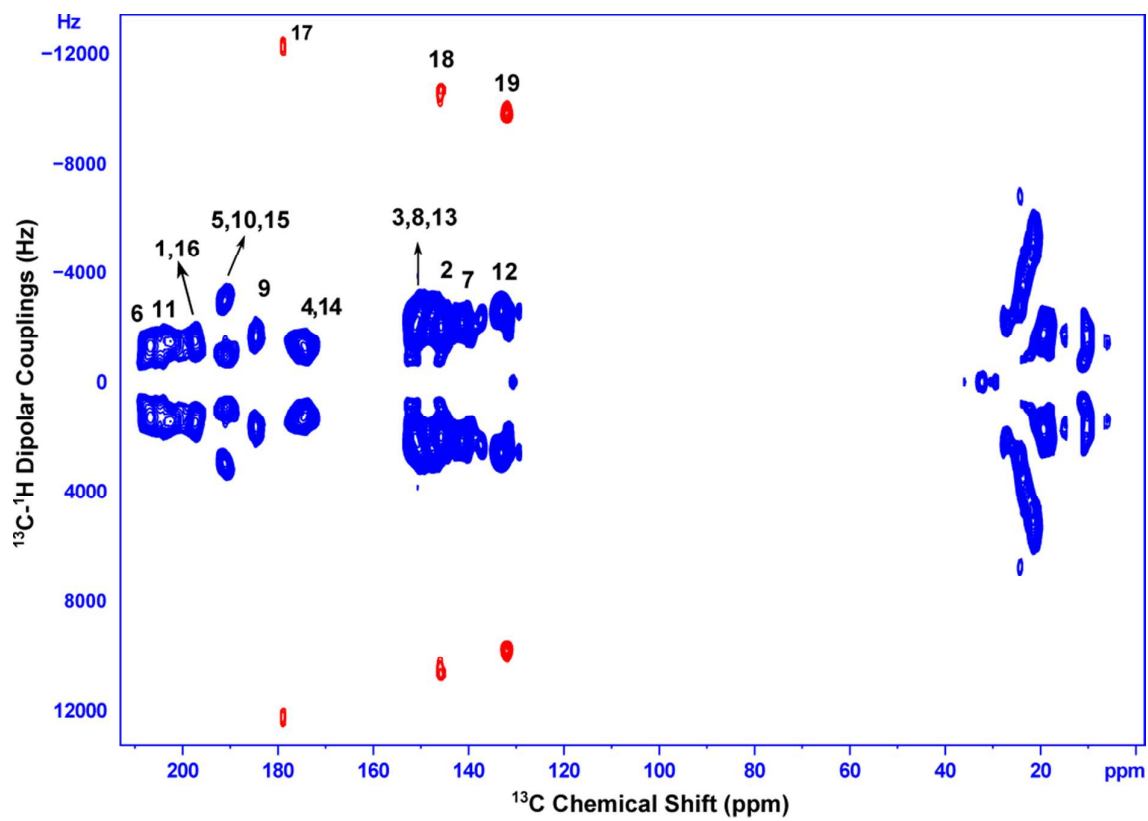


Figure 7



Kesava Reddy et al

Figure 8

